Strain Limiting for Soft Finger Contact Simulation

Alvaro G. Perez Gabriel Cirio Fernando Hernandez Carlos Garre Miguel A. Otaduy

URJC Madrid

ABSTRACT

The command of haptic devices for rendering direct interaction with the hand requires thorough knowledge of the forces and deformations caused by contact interactions on the fingers. In this paper, we propose an algorithm to simulate nonlinear elasticity under frictional contact, with the goal of establishing a model-based strategy to command haptic devices and to render direct hand interaction. The key novelty in our algorithm is an approach to model the extremely nonlinear elasticity of finger skin and flesh using strain-limiting constraints, which are seamlessly combined with frictional contact constraints in a standard constrained dynamics solver. We show that our approach enables haptic rendering of rich and compelling deformations of the fingertip.

Index Terms: I.2.9 [Robotics]—; I.3.7 [Three Dimensional Graphics and Realism]: Virtual Reality—

1 INTRODUCTION

To render high-fidelity haptic feedback of the interaction with simulated objects, the command and actuation of haptic devices must rely on a thorough understanding of the forces and deformations present at contact locations. In the case of haptic rendering of direct interaction with the hand, this implies the interactive computation of accurate forces and deformations at fingertips. Over the past, research on haptic rendering has produced excellent methods to support kinesthetic rendering of tool-based interaction, but in recent years we have also witnessed the invention of multiple cutaneous haptic devices, using a variety of technologies and skin stimulation principles [6, 29, 36, 32, 12, 5]. This progress in hardware design calls for novel methods to compute accurate forces and deformations on fingertips for cutaneous haptic rendering.

In this paper, we investigate a computationally efficient approach to simulate accurate soft finger contact. Our results are intended to be part of a model-based control strategy for haptic rendering of direct hand interaction, in which the forces and/or deformations needed to command the haptic device are computed by resolving the interaction between a finger model and simulated objects or materials. The computation of high-fidelity forces and deformations during finger contact is challenged by two major difficulties: frictional contact and the extreme nonlinear elasticity of finger skin.

We propose a novel method for the simulation of highly nonlinear tissue under frictional contact, based on the use of constrained optimization to model in a combined manner nonlinear elasticity and frictional contact. As shown in Section 3, we formulate nonlinear elasticity using strain-limiting constraints. This is an efficient alternative to hyperelastic models, and often the model of choice for highly nonlinear elasticity in computer graphics [28, 4, 34]. Our formulation supports bilateral or unilateral strain limiting, as well as isotropic or anisotropic strain limiting. These properties allow us to control independently the nonlinear elastic behavior under traction or compression, as well as on different directions.

In Section 4, we show how to integrate strain-limiting constraints with contact constraints in a unified constrained dynamics solver.

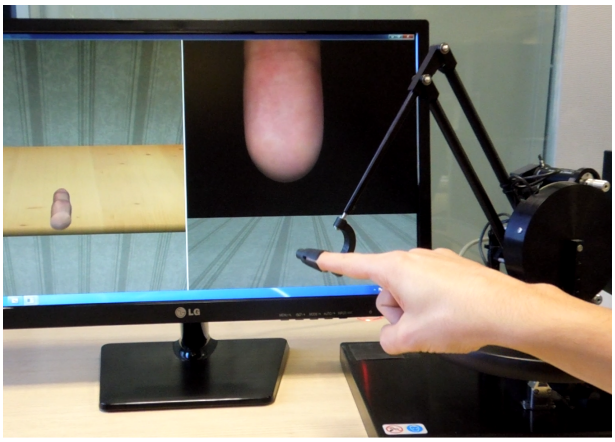

Figure 1: A user manipulates a haptic device with a thimble end-effector. The split screen shows, on the left, a first-person view of a finger model tapping a wooden table, and on the right, a close-up bottom view of the fingertip.

The overall simulation algorithm is simple and relies on standard solvers, allowing the solution of dynamics with robust implicit integration, constraint-based contact, and Coulomb friction. To display force feedback through a haptic device, we apply a modular approach that separates the simulation of the finger from the computation of feedback forces, and we connect both modules using a virtual coupling mechanism [8].

We have tested our simulation algorithm on different examples of soft tissue deformation, highlighting the diversity of nonlinear behaviors that can be achieved, and comparing the behavior to linear elastic materials. But most importantly, we have applied our algorithm to the simulation of soft finger contact with haptic feedback of direct finger interaction, as shown in Fig. 1. A human finger model is simulated while tracking the haptic device, and forces and deformations on the finger's skin are computed interactively to command the feedback forces of the haptic device.

2 RELATED WORK

Direct haptic interaction with the hand places important challenges on the simulation of hand biomechanics. The simulation must be computed at high frame rates for stable and high-fidelity haptic feedback, and it must accurately capture forces and deformations to send realistic commands to the haptic device.

Computer graphics solutions for hand animation focus on visual realism. Anatomically inspired biomechanical models [33] produce highly realistic animations, but are too computationally expensive for haptic rendering. Purely geometric methods [17, 19], on the other hand, do not support local skin deformations due to contact interactions. And some solutions leverage real data to simulate grasping realistically [27, 20, 18], but do not consider the deformation of the hand's skin under contact.

Several researchers have already addressed haptic interaction with an animated hand model, but the majority of the solutions ignore flesh deformation. One solution for haptic grasping considers

an articulated hand connected with springs for force feedback [3], another solution adds skinning to the skeleton [13], and another one includes a proxy-type skeleton with two-handed manipulation [24]. Ciocarlie et al. [7] included a localized soft finger contact model. Recently, Garre et al. [10] modeled a fully deformable hand coupled to an articulated skeleton. Their approach models the flesh as a linear elastic material, which is not capable of capturing the range of behaviors of the finger's skin.

Correct modeling of the finger tissue requires capturing nonlinear elasticity. We refer the reader to classic textbooks for detailed information on the topic [2, 14]. Commonly accepted elasticity models in computer animation include the linear corotational model [21] and the St. Venant-Kirchhoff model with nonlinear Green-Lagrange strain and a linear stress-strain relationship [15]. However, simulations of human tissue in computational mechanics resort to hyperelastic biologically-inspired models such as Ogden, Neo-Hookean or Mooney-Rivlin [22].

Nonlinear hyperelastic models come with drawbacks too. The finger is extremely nonlinear, particularly under compression. It is very compliant under light loading, but soon becomes almost rigid. In these conditions, hyperelastic models exhibit a very high numerical stiffness, which requires very small simulation time steps. Instead, we propose to model the extreme nonlinearity of the finger using strain-limiting constraints, which in essence eliminate degrees of freedom from the computations. Strain-limiting methods enable larger time steps, and they turn the complexity into the enforcement of constraints.

Strain-limiting was initially applied to cloth simulation based on the mass-spring model [28, 4], and later extended to finite element methods [34]. In the finite element setting, it requires the computation of principal strains for mesh elements, which are later constrained to predefined limits. Principal strains are also computed for the simulation of invertible hyperelastic materials [15], and gradients of principal strains are needed for robust implicit integration of such hyperelastic materials [31].

Typical strain-limiting solvers apply iterative relaxation locally on mesh elements until the object converges to a valid configuration. This process is analogous to Jacobi or Gauss-Seidel relaxation of a Lagrange-multipliers formulation with explicit integration. Instead, we propose a Lagrange-multiplier formulation with implicit integration, which makes the relaxation steps global. In other words, when locally resolving the strain of one mesh element, we transmit the deformation globally to the complete mesh, not just to the nodes of the element, improving the overall convergence. Wang et al. [35] extended the original method to improve the convergence of relaxation by following a multi-resolution scheme. In our approach, strain-limiting constraints are treated just like other constraints such as contact, and they can all be solved simultaneously using standard solvers.

3 Strain-Limiting Constraints

In this section, we present our formulation of nonlinear elasticity based on an underlyng linear elastic model augmented with strain-limiting constraints. We first present the formulation of continuum elasticity and its finite element discretization, and we follow with the formulation of strain-limiting constraints. We also describe the computation of constraint Jacobians, necessary for the constrained optimization solver.

3.1 Elastic Deformations

As the underlying elasticity model, we use a linear co-rotational strain formulation [21] with a (linear) Hookean material model. We discretize the continuum elasticity equations using the finite element method (FEM) and a tetrahedral mesh with linear basis functions. With these assumptions, the strain and stress tensors are constant inside each tetrahedral element.

Given the four nodes $\{\mathbf{x}_1,\mathbf{x}_2,\mathbf{x}_3,\mathbf{x}_4\}$ of a tetrahedral element, we define its volume matrix

$$\mathbf{X} = \begin{pmatrix} \mathbf{x}_1-\mathbf{x}_4 & \mathbf{x}_2-\mathbf{x}_4 & \mathbf{x}_3-\mathbf{x}_4 \end{pmatrix}. \tag{1}$$

For convenience, we express the inverse of the rest-state volume matrix based on its rows:

$$\mathbf{X}_0^{-1} = \begin{pmatrix} \mathbf{r}_1 \\ \mathbf{r}_2 \\ \mathbf{r}_3 \end{pmatrix}. \tag{2}$$

Using the volume matrix, the deformation gradient $\mathbf{G} = \frac{\partial \mathbf{x}}{\partial \mathbf{x}_0}$ of a tetrahedron can be computed as

$$\mathbf{G} = \mathbf{X}\mathbf{X}_0^{-1}. \tag{3}$$

The (linear) Cauchy strain tensor is defined based on the deformation gradient as

$$\varepsilon = \frac{1}{2}(\mathbf{G}+\mathbf{G}^T). \tag{4}$$

And a (linear) Hookean material can be defined by a linear stress-strain relationship of the form

$$\sigma = \mathbf{E}\,\varepsilon. \tag{5}$$

In our examples, we have used isotropic materials where the tensor $\mathbf{E}$ depends only on the Young modulus E and Poisson's ratio ν.

The continuum elasticity formulation defines elastic forces $\mathbf{f}$ from the stress field σ as $\mathbf{f}_{\text{elastic}} = \nabla \cdot \sigma$. With the FEM discretization, and concatenating all nodal positions in one large vector $\mathbf{x}$ and all nodal forces in one large vector $\mathbf{F}$, the elastic forces can be expressed as a linear function of positions, based on the stiffness matrix $\mathbf{K}$:

$$\mathbf{F}_{\text{elastic}} = -\mathbf{K}(\mathbf{x}-\mathbf{x}_0). \tag{6}$$

We apply the co-rotational strain formulation [21], in which a rotation matrix $\mathbf{R}_{\text{element}}$ is estimated per element, and the strain is measured in the unrotated setting. In practice, the co-rotational formulation amounts to warping the stiffness matrix of each element as $\mathbf{K}'_{\text{element}} = \mathbf{R}_{\text{element}}\,\mathbf{K}_{\text{element}}\,\mathbf{R}^T_{\text{element}}$.

3.2 Formulation of Strain-Limiting Constraints

For small deformations the finger tissue is very compliant. For such small deformations the linear elastic material described above captures well this compliance. However, the finger tissue soon becomes very stiff. This highly nonlinear behavior of the finger has been measured experimentally [30], and is depicted by the purple curve in the inset. We approximate this sudden stiffening effect using strain-limiting constraints, depicted in blue. The figure also compares compliant and stiff linear behaviors.

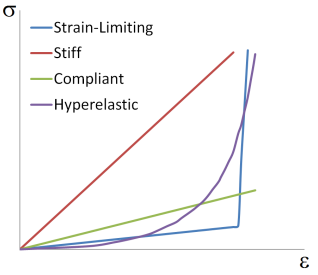

We limit strain effectively by limiting the deformation gradient of each tetrahedron in the finite element mesh. To this end, we compute a singular value decomposition (SVD) of the deformation gradient of each tetrahedron:

$$\mathbf{G} = \mathbf{U}\mathbf{S}\mathbf{V}^T \;\Rightarrow\; \mathbf{S} = \begin{pmatrix} s_1 & 0 & 0 \\ 0 & s_2 & 0 \\ 0 & 0 & s_3 \end{pmatrix} = \mathbf{U}^T\mathbf{G}\mathbf{V}, \tag{7}$$

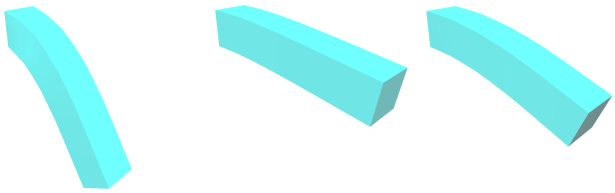

Figure 2: A deformed beam with three different materials. From left to right: linear-elastic with low elasticity ($E = 0.2$MPa), linear-elastic with higher elasticity ($E = 2$MPa), and strain-limiting ($E = 0.2$Mpa, $0.9 < s_i < 1.1$).

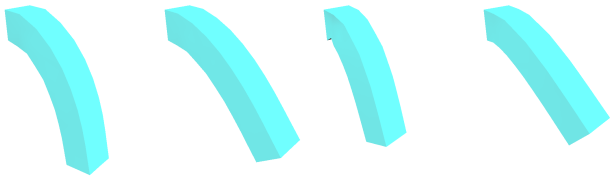

Figure 3: A beam under two different unilateral strain-limiting settings. Left: middle and final frame under compression limiting ($0.95 < s_i$). Right: middle and final frame under stretch limiting ($s_i < 1.05$). The Young modulus is $E = 80$kPa in both cases.

where the singular values $(s_1\ s_2\ s_3)$ capture deformations along principal axes. For convenience, we express the rotations $\mathbf{U}$ and $\mathbf{V}$ based on their columns:

$$\mathbf{U} = \begin{pmatrix} \mathbf{u}_1 & \mathbf{u}_2 & \mathbf{u}_3 \end{pmatrix}, \quad \mathbf{V} = \begin{pmatrix} \mathbf{v}_1 & \mathbf{v}_2 & \mathbf{v}_3 \end{pmatrix} \tag{8}$$

Unit singular values in all directions (i.e., $s_i = 1$) imply no deformation, while a unit determinant (i.e., $\det(\mathbf{G}) = s_1 s_2 s_3 = 1$) implies volume preservation. We enforce strain limiting by applying a lower limit $s_{\min}$ (i.e., compression constraint) and an upper limit $s_{\max}$ (i.e., stretch constraint) on each singular value of the deformation gradient:

$$s_{\min} \leq s_i \leq s_{\max}. \tag{9}$$

Fig. 2 compares linear-elastic materials with Young moduli of 0.2MPa and 2MPa vs. a linear material with Young modulus 0.2MPa and strain-limiting constraints of $s_{\min} = 0.9$ and $s_{\max} = 1.1$. With our formulation it is also very easy to choose between bilateral or unilateral strain limiting, or to apply anisotropic strain limiting. Fig. 3 shows examples of compression constraints but no stretch constraints, and stretch constraints but no compression constraints.

3.3 Constraint Jacobians

We enforce strain limiting constraints following a constrained optimization formulation described in the next section. This formulation requires the computation of constraint Jacobians w.r.t. the generalized coordinates of the system (i.e., the nodal positions of the finite element mesh) due to two reasons. First, constraints are nonlinear, and we locally linearize them in each simulation step. Second, we enforce constraints using the method of Lagrange multipliers, which applies forces in the direction normal to the constraints.

To define constraint Jacobians, we take for example one compression constraint of one tetrahedron (the formulation is analogous for stretch constraints):

$$C_i = s_i - s_{\min} \geq 0. \tag{10}$$

From the definitions of the deformation gradient in Eqs. (1)-(3) and its singular values in Eqs. (7)-(8), the Jacobians of the constraint w.r.t. the four nodes of the tetrahedron can be computed as:

$$\begin{aligned} \frac{\partial C_i}{\partial \mathbf{x}_j} &= \frac{\partial s_i}{\partial \mathbf{x}_j} = \mathbf{r}_j^T \mathbf{v}_i \mathbf{u}_i^T, \quad j \in \{1,2,3\} \\ \frac{\partial C_i}{\partial \mathbf{x}_4} &= \frac{\partial s_i}{\partial \mathbf{x}_4} = -(\mathbf{r}_1 + \mathbf{r}_2 + \mathbf{r}_3)^T \mathbf{v}_i \mathbf{u}_i^T. \end{aligned} \tag{11}$$

The derivation follows easily from the fact that $\frac{\partial s_k}{\partial g_{ij}} = u_{ik} v_{jk}$ [25].

In this section we have shown the formulation of strain-limiting constraints and their Jacobians based on the deformation gradient. The formulation can be extended to constraints defined on principal strains of the Cauchy strain tensor from Eq. (4) (or even the nonlinear Green-Lagrange strain tensor), with a slight complication of the Jacobians. In addition, expressing constraints based on principal strains allows a direct extension to other finite element discretizations, such as hexahedral meshes.

4 Simulation Algorithm and Haptic Rendering

In this section, we describe our algorithm for simulating deformation dynamics with strain limiting. We formulate the simulation as a constrained optimization problem, namely a linear complementarity problem, and we apply standard solvers. We start the section with a description of unconstrained dynamics, and then we add strain-limiting constraints and contact constraints with friction. We conclude by discussing the addition of haptic feedback following also standard coupling mechanisms.

4.1 Constrained Dynamics

The unconstrained dynamics of deformable bodies can be expressed in matrix form as $\mathbf{M}\dot{\mathbf{v}} = \mathbf{F}$, where $\mathbf{v}$ is a vector that concatenates all nodal velocities, $\mathbf{F}$ is a vector with all nodal forces, including gravity, elasticity, etc., and $\mathbf{M}$ is the mass matrix. Given positions $\mathbf{x}_0$ and velocities $\mathbf{v}_0$ at the beginning of a simulation step, we integrate the equations with backward Euler implicit integration and linearized forces, which amounts to solving the following linear system:

$$\begin{aligned} \mathbf{A}\mathbf{v}^* = \mathbf{b}, \quad \text{with } \mathbf{A} &= \mathbf{M} - h\frac{\partial \mathbf{F}}{\partial \mathbf{v}} - h^2 \frac{\partial \mathbf{F}}{\partial \mathbf{x}} \\ \text{and } \mathbf{b} &= \left(\mathbf{M} - h\frac{\partial \mathbf{F}}{\partial \mathbf{v}}\right)\mathbf{v}_0 + h\mathbf{F}. \end{aligned} \tag{12}$$

We denote with h the size of the simulation step.

With these unconstrained velocities $\mathbf{v}^*$, we integrate positions $\mathbf{x}^* = \mathbf{x}_0 + h\mathbf{v}^*$, and check whether strain-limiting constraints are violated. We group all constraints in one large vector $\mathbf{C}$, and linearize them at the beginning of the simulation step ($\mathbf{C}_0$), using the generalized constraint Jacobian $\frac{\partial \mathbf{C}}{\partial \mathbf{x}} = \mathbf{J}$:

$$\mathbf{J}\mathbf{v} \geq -\frac{1}{h}\mathbf{C}_0. \tag{13}$$

The constrained dynamics problem is a quadratic program (QP) that consists of finding the closest velocity to the unconstrained one, subject to the constraints, i.e.,

$$\mathbf{v} = \arg\min(\mathbf{v} - \mathbf{v}^*)^T \mathbf{A}(\mathbf{v} - \mathbf{v}^*), \quad \text{s.t. } \mathbf{J}\mathbf{v} \geq -\frac{1}{h}\mathbf{C}_0. \tag{14}$$

This QP is equivalent to the following linear complementarity problem (LCP):

$$0 \leq \lambda \quad \perp \quad \mathbf{J}\mathbf{A}^{-1}\mathbf{J}^T\lambda + \mathbf{J}\mathbf{A}^{-1}\mathbf{b} + \frac{1}{h}\mathbf{C}_0 \geq 0. \tag{15}$$

with constrained velocities computed as

$$\mathbf{A}\mathbf{v} = \mathbf{b} + \mathbf{J}^T\lambda. \tag{16}$$

Figure 4: Simulation of a bunny (density $\rho = 1000\text{kg/m}^3$) using: (left) a very compliant linear material with $E = 30\text{kPa}$, (middle) a stiffer linear material with $E = 60\text{kPa}$, and (right) the compliant material with a stretch limit of $s_i < 1.1$. With our approach, the ears of the bunny remain similar to the stiff material, but the body retains its compliance under small deformations.

In our examples, we solve the LCP using projected Gauss-Seidel (PGS) relaxation [9].

4.2 Contact and Friction

Given two points $\mathbf{p}_a$ and $\mathbf{p}_b$ defining a collision, and the outward normal $\mathbf{n}_b$ at $\mathbf{p}_b$, we formulate a non-penetration constraint as

$$C = \mathbf{n}_b^T(\mathbf{p}_a - \mathbf{p}_b) \geq 0. \tag{17}$$

Non-penetration constraints are linearized as in Eq. (13), added to the vector of constraints $\mathbf{C}$ together with strain-limiting constraints, and solved simultaneously.

We incorporate contact friction using Coulomb's model. In practice, in each iteration of PGS, after the normal force of a contact λ_n is computed, we add friction forces λ_t in the tangent plane of contact. To compute the forces, we maximize the dissipation of tangential velocity subject to the Coulomb cone constraint, $\|\lambda_t\| \leq \mu\,\lambda_n$, where μ is the friction coefficient. We approximate the cone constraint using a four-sided pyramid.

4.3 Error Metrics

The algorithm described in Section 4.1 above is a standard approach for simulating dynamics under non-penetration contact constraints [16, 23]. Then, the simultaneous simulation of strain-limiting and contact constraints is simply carried out by merging strain-limiting constraints of the form (10) and contact constrains of the form (17) into the same set of constraints $\mathbf{C}$.

However, the convergence of the PGS solver for the LCP in Eq. (15) requires appropriate weighting of the various constraint errors. We measure the error of the constrained problem as

$$\text{error} = \sum_i w_i \|\min(C_i, 0)\|. \tag{18}$$

To weight the constraints, we simply express constraint errors as distances in the units of the workspace. Contact constraints as in Eq. (17) are already expressed in distance units; therefore, we set $w_i = 1$ for them. Strain-limiting constraints as in Eq. (10) are dimensionless and indicate a relative scaling of tetrahedra. To transform them to distance units, we scale each strain-limiting constraint by the average edge length e of its corresponding tetrahedron, i.e., $w_i = e$.

4.4 Haptic Coupling

In our current implementation, we provide haptic interaction through kinesthetic devices. To couple the device and the simulation, we follow a virtual coupling approach [8]. The complete deformable finger plays the role of *haptic tool*, and to couple the haptic device we associate a rigid *haptic handle* to the finger [10]. The handle is connected to the haptic device through a virtual coupling mechanism. We initialize the haptic handle with the same size, mass, and position as the finger, and we connect the tool and handle using springs, which provide bi-directional coupling.

In our current implementation, we simulate the finger model in a *visual thread*, whose frame rate is limited by the simulation updates. To improve the quality of haptic feedback, we simulate a proxy handle in a *haptic thread* running at 1kHz, and we set up virtual coupling mechanisms between the handle and its proxy, and the proxy and the haptic device. Further improvements to haptic feedback could be possible by substituting the virtual coupling between the handle and the proxy with a handle-space linearization of the spring forces between the handle and the tool [10].

To test our simulation algorithm, we have used two haptic devices. As shown in Fig. 1, a Phantom Premium with a thimble-type end-effector provides direct kinesthetic feedback on the fingertip. However, the thimble-type end-effector lacks tracking of orientations, and to test our model under full 6-DoF tracking we have also integrated the simulation with a Phantom Omni haptic device.

5 Results and Evaluation

In this section, we present a set of simulation scenarios to illustrate and qualitatively assess our strain-limiting approach. Simulations were run on a 3.4 GHz Quad-core Intel Core i7-3770 CPU with 32GB of memory.

5.1 Animation Tests

In order to qualitatively test the effect of strain limiting, we ran different simulations with a 1m $\times$ 0.2m $\times$ 0.2m beam, fixed at one of its ends, with 200 tetrahedra and a mass density of 1,000 Kg/m^3. Fig. 3 shows the beam under two different unilateral strain-limiting settings, namely compression and stretch limits, with a Young modulus of 80kPa. Fig. 2 shows the beam with three different materials: compliant linear-elastic (E =0.2MPa), stiffer linear-elastic(E = 2MPa) and compliant strain limiting (E =0.2MPa). The example also illustrates that the strain-limiting approach suffers higher numerical damping, due to the projection of the deformation onto the constraint limits.

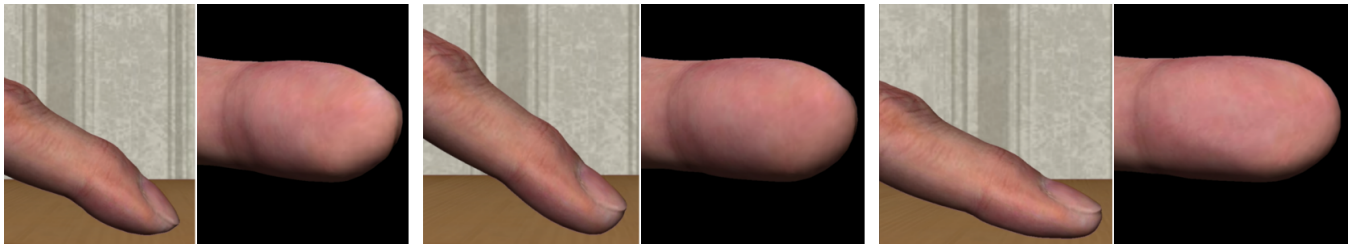

Figure 5: Three screen captures (side and bottom views) of interactive deformations of a finger model under frictional contact, with unconstrained (reference, middle), backward (left) and forward (right) motions of the finger. The finger was simulated with a Young modulus of 2,000 kPa and isotropic strain-limiting of $0.9 < s_i < 1.1$.

We also tested our method on more complex animation models. Fig. 4 shows a bunny model (approx. 25cm high, density $\rho = 1000\text{kg/m}^3$, 5,812 tetrahedra) simulated with different material properties. We compared a very compliant linear material ($E = 30\text{kPa}$), a stiffer linear material ($E = 60\text{kPa}$), and the compliant material with a stretch limit of $s_i < 1.1$. With the compliant material the body shows interesting jiggling, but the ears collapse. With the stiff material, on the other hand, the ears remain high, but the body deforms little. With our approach, the ears remain similar to the stiff material and the body retains its compliance under small deformations.

5.2 Haptic Rendering of Finger Contact

To illustrate our strain-limiting approach in the context of haptic rendering of direct finger contact, and compare it to a linear material model, we simulated a set of simple interaction scenarios. We used a finger model of approximately 7cm with 347 tetrahedra, simulated with a mass density of 1,000 Kg/m^3, a Young modulus of 2MPa and isotropic strain-limiting of $0.9 < s_i < 1.1$. Haptic interaction was performed through a 6-DoF-input/3-DoF-output Phantom Omni haptic device and a 3-DoF-input/3-DoF-output thimble-type Phantom Premium, as described in Section 4.4.

When under unconstrained motion, the simulation ran at an average frequency of 320Hz. During contact and friction scenarios such as those illustrated in Fig. 5 and Fig. 6, strain limiting constraints were activated in up to 60 tetrahedra per simulation step. The simulation frequency remained higher than 40Hz even under highly constrained situations, and was in the order of 100Hz for normal interactions. Higher frequencies could be achieved adopting a multirate approach [11, 26].

Fig. 5 shows screen captures of unconstrained (reference, middle), backward (left) and forward (right) motions of the finger under frictional contact with a table. The fingertip is deformed in a realistic way, stretching and bulking the tissue, while preventing the common limitations of linear models. These limitations are visible in Fig. 6, with inversion of tetrahedra (top left) during sliding frictional motions and collapse due to excessive compression (bottom left) during pressing motions. The correct results using our strain-limiting approach are shown on the right side of the same figure.

These results could have a strong impact on haptic rendering of direct hand interaction too. In a model-based control strategy to command tactile devices, it is important to compute realistic contact variables such as contact area, friction, force magnitude, and force distribution. We have compared contact variables with a linear elastic model and our strain-limiting approach in an experiment where the full finger is pressed flat against a plane. Fig. 5 shows plots of the total normal contact force vs. the total contact area for the two models. Our strain-limiting approach shows the expected fast increase of the contact force once a certain contact area is reached. The stair-case profiles are due to the discretization of the contact surface.

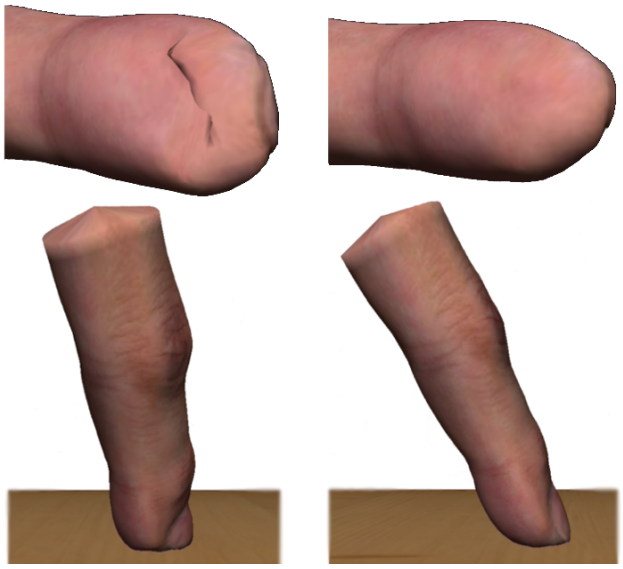

Figure 6: As shown on the left, the finger suffers severe artifacts when we use a compliant linear material. On top, bottom view of flipped tetrahedra due to friction forces, and on the bottom, side view of collapsed finger under pressing forces. As shown on the right, these situations are robustly handled with our strain-limiting model.

6 Discussion and Future Work

In this paper, we have presented a model for simulating highly nonlinear elastic deformations using strain-limiting constraints. Our model enables the interactive simulation of a finger model with nonlinear elasticity and frictional contact, showing rich and robust deformations during haptic interaction. The core novelty of the method is a formulation of constrained dynamics with unified handling of strain-limiting and contact constraints.

For the examples presented in the paper, the stiffness and strain-limiting of the finger were set as uniform parameters for the complete model and were tuned ad-hoc. The quality of the deformations would increase by setting heterogeneous material properties and estimating them automatically from real-world measurements [1].

As mentioned in the introduction, our work was largely motivated by the use of an accurate finger simulation as a model-based control strategy in the command of cutaneous haptic devices. Currently, we have successfully tested the simulation with kinesthetic haptic devices, and we plan to test it as well with cutaneous devices. To this end, it is important to identify the particular forces and/or deformations needed to command specific cutaneous devices.

Our work can be extended and improved in several other ways.

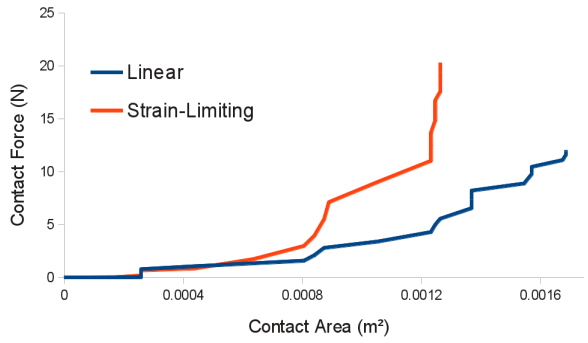

Figure 7: Total contact force vs. total contact area for a linear elastic model (blue) and our strain-limiting approach (red), when a finger is pressed flat against a plane.

For instance, the performance of the simulation is currently limited by the projected Gauss-Seidel solver of the constrained optimization. Finding more efficient solvers would allow the simulation of higher-resolution models interactively, with the possibility to render more detailed haptic feedback. In our work, we have focused on the improvement of the elastic behavior of finger simulation models, but accurate modeling of the finger can leverage additional recent findings about its mechanical behavior [37]. Last, as we show in the paper our model is not limited to simulating the finger, and we plan to apply it to the simulation of larger body parts.

Acknowledgements

This work was supported in part by grants from the Spanish Ministry of Economy (TIN2009-07942, TIN2012-35840), the European Research Council (ERC-2011-StG-280135 Animetrics), and the EU FP7 project WEARHAP (601165).

References

[1] B. Bickel, M. Bächer, M. A. Otaduy, W. Matusik, H. Pfister, and M. Gross. Capture and modeling of non-linear heterogeneous soft tissue. *ACM Trans. Graph.*, 28(3):89:1–89:9, July 2009.

[2] J. Bonet and R. D. Wood. *Nonlinear Continuum Mechanics for Finite Element Analysis*. Cambridge University Press, 1997.

[3] C. W. Borst and A. P. Indugula. Realistic virtual grasping. In *Proc. of IEEE Virtual Reality Conference*, 2005.

[4] R. Bridson, S. Marino, and R. Fedkiw. Simulation of clothing with folds and wrinkles. *Proc. of ACM SIGGRAPH / Eurographics Symposium on Computer Animation*, 2003.

[5] F. Chinello, M. Malvezzi, C. Pacchierotti, and D. Prattichizzo. A three dofs wearable tactile display for exploration and manipulation of virtual objects. In *IEEE Haptics Symposium*, 2012.

[6] E. Chubb, J. Colgate, and M. Peshkin. ShiverPaD: a glass haptic surface that produces shear force on a bare finger. *IEEE Transactions on Haptics*, 3(3):189 –198, 2010.

[7] M. Ciocarlie, C. Lackner, and P. Allen. Soft finger model with adaptive contact geometry for grasping and manipulation tasks. In *World Haptics Conference*, 2007.

[8] J. E. Colgate, M. C. Stanley, and J. M. Brown. Issues in the haptic display of tool use. *Proc. of IEEE/RSJ International Conference on Intelligent Robots and Systems*, pages pp. 140–145, 1995.

[9] R. Cottle, J. Pang, and R. Stone. *The Linear Complementarity Problem*. Academic Press, 1992.

[10] C. Garre, F. Hernandez, A. Gracia, and M. A. Otaduy. Interactive simulation of a deformable hand for haptic rendering. In *Proc. of World Haptics Conference*, 2011.

[11] C. Garre and M. A. Otaduy. Haptic rendering of complex deformations through handle-space force linearization. In *Proc. of World Haptics Conference*, mar 2009.

[12] B. Gleeson, C. Stewart, and W. Provancher. Improved tactile shear feedback: Tactor design and an aperture-based restraint. *IEEE Transactions on Haptics*, 4(4):253 –262, 2011.

[13] X. Han and H. Wan. A framework for virtual hand haptic interaction. In *Transactions on Edutainment IV*, 2010.

[14] G. A. Holzapfel. *Nonlinear Solid Mechanics: A Continuum Approach for Engineering*. Wiley, 2000.

[15] G. Irving, J. Teran, and R. Fedkiw. Invertible finite elements for robust simulation of large deformation. *Proc. of ACM SIGGRAPH/Eurographics Symposium on Computer Animation*, pages 131–140, 2004.

[16] D. M. Kaufman, S. Sueda, D. L. James, and D. K. Pai. Staggered projections for frictional contact in multibody systems. *Proc. of ACM SIGGRAPH Asia*, 2008.

[17] P. G. Kry, D. L. James, and D. K. Pai. Eigenskin: Real time large deformation character skinning in hardware. In *ACM SIGGRAPH Symposium on Computer Animation*, pages 153–160, July 2002.

[18] P. G. Kry and D. K. Pai. Interaction capture and synthesis. *ACM Transactions on Graphics*, 25(3):872–880, July 2006.

[19] T. Kurihara and N. Miyata. Modeling deformable human hands from medical images. In *2004 ACM SIGGRAPH / Eurographics Symposium on Computer Animation*, pages 355–363, July 2004.

[20] Y. Li, J. L. Fu, and N. S. Pollard. Data-driven grasp synthesis using shape matching and task-based pruning. *IEEE Transactions on Visualization and Computer Graphics*, 13(4):732–747, July/Aug. 2007.

[21] M. Müller and M. Gross. Interactive virtual materials. *Proc. of Graphics Interface*, 2004.

[22] R. W. Ogden. *Non-Linear Elastic Deformations*. Courier Dover Publications, 1997.

[23] M. A. Otaduy, R. Tamstorf, D. Steinemann, and M. Gross. Implicit contact handling for deformable objects. *Computer Graphics Forum*, 28(2):559–568, Apr. 2009.

[24] R. Ott, F. Vexo, and D. Thalmann. Two-handed haptic manipulation for CAD and VR applications. *Computer Aided Design & Applications*, 7(1), 2010.

[25] T. Papadopoulo and M. I. A. Lourakis. Estimating the jacobian of the singular value decomposition: Theory and applications. In *European Conference on Computer Vision*, 2000.

[26] I. Peterlik, M. Nouicer, C. Duriez, S. Cotin, and A. Kheddar. Constraint-based haptic rendering of multirate compliant mechanisms. *IEEE Transactions on Haptics*, 4(3):175 –187, 2011.

[27] N. S. Pollard and V. B. Zordan. Physically based grasping control from example. In *2005 ACM SIGGRAPH / Eurographics Symposium on Computer Animation*, pages 311–318, July 2005.

[28] X. Provot. Deformation constraints in a mass-spring model to describe rigid cloth behavior. *Proc. of Graphics Interface*, 1995.

[29] E. Scilingo, M. Bianchi, G. Grioli, and A. Bicchi. Rendering softness: Integration of kinesthetic and cutaneous information in a haptic device. *IEEE Transactions on Haptics*, 3(2):109 –118, 2010.

[30] E. R. Serina, C. D. Mote, and D. Rempel. Force response of the fingertip pulp to repeated compression: Effects of loading rate, loading angle and anthropometry. *Journal of Biomechanics*, 30(10), 1997.

[31] F. Sin, Y. Zhu, Y. Li, D. Schroeder, and J. Barbič. Invertible isotropic hyperelasticity using SVD gradients. In *ACM SIGGRAPH / Eurographics Symposium on Computer Animation (Posters)*, 2011.

[32] M. Solazzi, W. Provancher, A. Frisoli, and M. Bergamasco. Design of a SMA actuated 2-DoF tactile device for displaying tangential skin displacement. In *IEEE World Haptics Conference*, 2011.

[33] S. Sueda, A. Kaufman, and D. K. Pai. Musculotendon simulation for hand animation. *ACM Trans. Graph.*, 27(3), Aug. 2008.

[34] B. Thomaszewski, S. Pabst, and W. Strasser. Continuum-based strain limiting. *Computer Graphics Forum*, 28(2):569–576, 2009.

[35] H. Wang, J. O'Brien, and R. Ramamoorthi. Multi-resolution isotropic strain limiting. *Proc. of ACM SIGGRAPH Asia*, 2010.

[36] Q. Wang and V. Hayward. Biomechanically optimized distributed tactile transducer based on lateral skin deformation. *Int. J. Rob. Res.*, 29(4):323–335, 2010.

[37] M. Wiertlewski and V. Hayward. Mechanical behavior of the fingertip in the range of frequencies and displacements relevant to touch. *Journal of Biomechanics*, 2012.